



# Lawrence Berkeley Laboratory

UNIVERSITY OF CALIFORNIA

## Materials & Molecular Research Division

Submitted to Metallurgical Transactions

THE MECHANICAL STABILITY OF PRECIPITATED AUSTENITE  
IN 9Ni STEEL

B. Fultz and J.W. Morris, Jr.

June 1985

**TWO-WEEK LOAN COPY**  
*This is a Library Circulating Copy  
which may be borrowed for two weeks.*



LBL-19499  
e.2

## **DISCLAIMER**

This document was prepared as an account of work sponsored by the United States Government. While this document is believed to contain correct information, neither the United States Government nor any agency thereof, nor the Regents of the University of California, nor any of their employees, makes any warranty, express or implied, or assumes any legal responsibility for the accuracy, completeness, or usefulness of any information, apparatus, product, or process disclosed, or represents that its use would not infringe privately owned rights. Reference herein to any specific commercial product, process, or service by its trade name, trademark, manufacturer, or otherwise, does not necessarily constitute or imply its endorsement, recommendation, or favoring by the United States Government or any agency thereof, or the Regents of the University of California. The views and opinions of authors expressed herein do not necessarily state or reflect those of the United States Government or any agency thereof or the Regents of the University of California.

# **THE MECHANICAL STABILITY OF PRECIPITATED AUSTENITE IN 9Ni STEEL**

**B. Fultz and J. W. Morris, Jr.**

Materials and Molecular Research Div., Lawrence Berkeley Laboratory,  
and the  
Dept. of Materials Science and Mineral Engineering,  
University of California, Berkeley, CA 94720

## **ABSTRACT**

The strains inherent to the martensitic transformation of austenite particles in 9Ni steel create dislocation structures in the tempered martensite. These dislocation structures were studied by the complementary techniques of x-ray line profile analysis and transmission electron microscopy. The energy required to form these dislocation structures affects the thermodynamics of the transformation. We propose that changes in these dislocation structures reduce the "mechanical stability" of the austenite particles as they grow larger during isothermal tempering.

## I. INTRODUCTION

In a previous paper, [1], we reported a detailed study of the stability of precipitated austenite against the martensitic transformation and how this stability is related to the ductile-to-brittle transition of 9Ni steel. In essence, the reduction in stability of the austenite during isothermal tempering leads to an increase in the ductile-to-brittle transition temperature. Microstructural features which affect the austenite stability were examined. Changes in the chemical composition of the austenite during tempering were too small to account for the large reduction in the stability of the austenite; the reduction in carbon concentration could account for a change in  $M_D$  of only 50°C, and the increasing Ni concentration of the austenite should actually stabilize the austenite with further tempering. Another microstructural feature which may affect the austenite stability is the coherency of the austenite/martensite interface. The energetics associated with the reduction in interface coherency during tempering are rather small. However, the nucleation of the transformation of an austenite particle may be influenced by changes in the dislocation structure at its surface. Such an effect is difficult to estimate quantitatively, and furthermore it may be true that the loss of interface coherency during tempering is a consequence, rather than a cause of the transformation of austenite particles.

In this paper we explore a third microstructural feature which affects the mechanical stability of austenite particles. This feature affects the mechanical stability of austenite particles as they transform to martensite. Detailed observations of these dislocation structures around fresh martensite particles are reported in this paper, and we show how changes in these dislocation structures reduce the austenite stability during isothermal tempering. We propose that the energy of formation of these dislocation structures is the basis for the "mechanical stability" of austenite particles.

## II. EXPERIMENTAL DATA ANALYSIS

Experimental techniques for material preparation and characterization were described in ref. [1]. In this section we describe further analysis of the x-ray diffraction lineshapes. We show how this analysis provides information about the dislocation structures which result from the transformation of austenite particles.

The broadening of both austenite and martensite x-ray diffraction peaks was analyzed to provide information on the internal strain distributions, and the average size of the coherently diffracting domains. The "method of multiple orders" due to Warren and Averbach [2-4] was unfeasible for this analysis because of the large number of specimens involved and the long counting times required for the high order peaks. Instead, the following method was used: A Rachinger correction [5] was performed to remove the  $K\alpha_2$  component of each peak. Instrument lineshapes were obtained from a large-grained (50  $\mu\text{m}$ ) austenitic specimen of a binary Fe-31Ni alloy annealed at 1100°C and slowly cooled. Appropriate instrument lineshapes were then deconvolved [6] from each peak with a fast Fourier transform method. The statistical scatter in the

experimental data contributed excessive amplitude to the higher order Fourier coefficients. To prevent divergence of the inverse Fourier transform, the transform of the peak divided by the transform of the instrument lineshape was multiplied by a Gaussian function to smoothly suppress the high order coefficients.

In the next section we show why diffraction peaks from a distribution of small diffracting domains tend to have a Lorentzian profile. Strain distributions in polycrystalline metals have been successfully described by Gaussian functions [2-4]. In general, we expect the presence of both small diffracting domains and an internal strain distribution, so we expect a diffraction profile that is the convolution of a Lorentzian function and a Gaussian function. The tails of a Lorentzian function are much stronger ( $\sim 1/x^2$ ) than the tails of a Gaussian function ( $\sim \exp(-x^2)$ ). Therefore, in separating size broadening from strain broadening, the Rachinger and Stokes-corrected peaks were fit to a numerical convolution of Gaussian and Lorentzian functions, with emphasis on the quality of fit in the tail regions of the peak. The data of Fig. 1 illustrate the method. Peak "a" was resolved into 65% Gaussian and 35% Lorentzian components, peak "b" was 25% Gaussian and 75% Lorentzian, and peak "c" was 10% Gaussian and 90% Lorentzian. We estimate the error in these assignments to be  $\pm 5\%$ , to which we add an uncertainty in the total width of the corrected peak in order to estimate the total error in the strain and size broadening data.

#### A. Theory of XRD Peak Shapes

The origin of the Lorentzian tails in x-ray diffraction lineshapes results from the distribution of small domain sizes in a manner proposed by Khachaturyan [7]. His argument is based on the probability,  $P(\ell)$ , of not finding a boundary to a column of atomic planes up to the distance,  $\ell$ , where the other end of the column is assumed to be at the origin. The probability that a given column will be terminated in the distance  $d\ell$  is  $\alpha(\ell)d\ell$ , so we have the relations between  $P(\ell)$  and  $\alpha(\ell)$ :

$$P(\ell) = P(\ell - d\ell) \cdot [1 - \alpha(\ell) \cdot d\ell], \quad 1)$$

$$dP = -P(\ell) \cdot \alpha(\ell) \cdot d\ell. \quad 2)$$

The probability,  $g(\ell) \cdot d\ell$ , of finding a column with a length between  $\ell$  and  $\ell + d\ell$  will be  $P(\ell)$  times  $\alpha(\ell) \cdot d\ell$ . Equation 2 has a simple exponential solution for  $P(\ell)$  when  $\alpha(\ell)$  is a constant, so the probability distribution for column lengths is:

$$g(\ell) = \frac{1}{\langle \ell \rangle} \cdot \exp \frac{-\ell}{\langle \ell \rangle}. \quad 3)$$

The Fourier transformation of Eqn. 3 gives a Lorentzian function for the XRD peak shapes. The boundaries and regions of high dislocation density that we have identified in TEM micrographs (see below) show many different separations, but we have not observed enough of them to compile statistics on their distributions. Perhaps the best justification that  $\alpha(\ell)$  is a constant (equal to  $\langle \ell \rangle^{-1}$ ) is that XRD peaks from over-tempered and cold-worked material have a Lorentzian-like profile. This approach predicts that the full-width-at-half-maximum (FWHM) of the

Lorentzian components, when linearized in k-space by multiplying by the factor  $\cos(\theta)$ , should be independent of the order of reflection. In fact, the corrected widths of the Lorentzian components of the martensite peaks did not increase significantly with the modulus of the diffraction vector. The Lorentzian component widths of the austenite peaks, however, showed a small tendency to scale with the modulus of the diffraction vector.

Nevertheless, the assumption that  $\alpha(\ell)$  is independent of  $\ell$  requires further discussion. When the dislocations are tightly formed into cell walls of random separation, the Khachaturyan approach applies for most of the material in the cell interiors. Wilkens [8] has approached the problem of x-ray line broadening in plastically deformed material with a direct theoretical treatment of elastic strain fields around dislocations. The range of elastic distortions from dislocations in the cell walls is small, and the size distribution of the cell interiors will produce a Lorentzian diffraction profile with its broad tails. Additional intensity in the tail region will arise from x-ray diffraction by the material in the cell walls. However, when the dislocations are more homogeneously distributed throughout the material, their elastic distortions extend over a longer range, and  $\alpha(\ell)$  tends to become linear in  $\ell$ . The shape of the diffraction profile tends towards a Gaussian function [8,9]. Our association of Lorentzian components of the XRD profile with dislocation distributions is therefore less appropriate when the dislocations are more homogeneously distributed throughout the material.

### B. Analysis of XRD Peak Shapes

The width of the strain distribution,  $\Delta s$ , was determined from the FWHM of the Gaussian component of the Rachinger and Stokes corrected peak shape,  $G(\theta)$ , with  $\theta$  in radians, by using the relationship:

$$\Delta s(\theta) = \cot(\theta) \cdot G(\theta) \quad . \quad 4)$$

The widths of the strain distributions in the austenite and the martensite are shown in Fig. 2 as a function of tempering time. The (220) $\gamma$  and (311) $\gamma$  peaks, and the (200) $\alpha'$  and (211) $\alpha'$  peaks were averaged for presentation in Fig. 2. Some systematic errors of 10-20% in strain distribution are expected from our method of data processing. Nevertheless, our strain distribution data for martensite seems roughly consistent with data from a HSLA steel that were obtained by the method of multiple orders [10]. For all materials the strain distribution in the austenite was about twice as large as the strain distribution in the martensite (see Fig. 2), and remain essentially constant with tempering. Cold rolling had no effect on the widths of the strain distributions. Immersion in liquid nitrogen had a small (and perhaps insignificant) effect on only the overtempered material. Error bars are drawn to indicate our overall confidence in the data of Figs. 2 and 3. Our confidence in the trends in particle size data (Fig. 3) is greater than our confidence in the trends in strain distribution data (Fig. 2) because the changes in peak broadening due to size effects were larger.

The average sizes of the diffracting domains were determined from the Scherrer approximation for a column of coherently diffracting planes of length  $\ell$  [3]:

$$l = \frac{\lambda}{L(2\theta) \cdot \cos(\theta)} \quad . \quad 5)$$

Here  $L(2\theta)$  is the FWHM of the Lorentzian component of the diffraction peak in radians, and  $\lambda$  is the x-ray wavelength. The average sizes of diffracting domains of the austenite and martensite are shown as a function of tempering time in Fig. 3. The austenite sizes are presented as an average of data from the  $(220)\gamma$  and  $(311)\gamma$  peaks, which showed very similar behavior. The average martensite sizes extracted from the  $(200)\alpha'$  peaks and the  $(211)\alpha'$  peaks are averaged for presentation in Fig. 3.

### III. RESULTS

The increase in size that is shown for the austenite over the first ten hours of tempering (see Fig. 3) is consistent with the growth in size of the austenite particles seen in TEM micrographs [1]. With further tempering, however, the mean sizes of x-ray diffracting domains are reduced, and this does not correspond to decreased dimensions of austenite particles or martensite laths observed with TEM. This reduction is slight between 10 and 100 hrs of tempering. However, the abrupt reduction in mean size of diffracting domains that occurs after 100 hrs of tempering is unmistakable. Immersion in liquid nitrogen had no effect on the average size of the austenite or martensite of material tempered less than 100 hrs. However, liquid nitrogen immersion resulted in a 20% reduction in austenite size for material tempered for more than 100 hrs. Liquid nitrogen immersion also caused a 5-10% reduction in martensite size for the material tempered for 750 hrs. A similar reduction in average size of the martensite and austenite was always produced by cold rolling at room temperature. These reductions in size of the austenite and the martensite diffracting domains correlated with the martensitic transformation of some of the austenite. The greater the extent of the transformation, the greater the reduction in size of coherently diffracting domains.

We first tried to explain these large reductions in average size of martensite diffracting domains by assuming a small effective size for only the fresh martensite and the tempered martensite immediately around it. This seemed reasonable because TEM micrographs showed that these regions of martensite have a very defective crystal structure. Accordingly, we tried to fit these broadened martensite diffraction profiles to a sum of two functions. The first function was attributed to the tempered martensite and had a narrow lineshape comparable to that of Fig. 1a. The second function, which had 10-15% of the integrated intensity of the first, was attributed to the defective martensite and had a broad Lorentzian lineshape of adjustable width. The quality of fit to the experimental peaks was clearly worse than the fit to a single convolution of a Gaussian and a Lorentzian function. We conclude that the large reduction in average size of the martensite diffraction domains reflects bulk changes in the tempered martensite, and not just the defect structure of a small amount of the martensite.

Figure 4 (and Figs. 6, 9 of [1]) shows the dislocation structure around partially transformed fresh martensite particles in material tempered for 300 hrs. The dislocations around the particles appear to

be forming into dislocation walls, but this process is incomplete. A smaller fresh martensite particle from 81 hr tempered material is shown in Fig. 5. The dense mesh of dislocations near the surface of the particle is present, but there is little disturbance of the tempered martensite away from the particle. A bright field TEM micrograph of material tempered for 3 hr and then given 25% cold work is shown in Fig. 6. A dense dislocation structure is seen around a martensite lath in the upper left corner of the figure, and a partially-formed dislocation wall structure is seen in the lower right. The average size of austenite and martensite diffracting domains (see Fig. 3) also shows a reduction after cold rolling which is comparable to the reduction after tempering for more than 100 hrs.

The large reduction in average size of the martensite diffraction domains after some of the austenite has transformed is due to the dislocation structures that radiate outwards from the fresh martensite and across the tempered martensite (see Fig. 4, and Figs. 6 and 9 of [1]). The average size of martensite diffraction domains for material tempered for 240 hrs is 530 Å. This is comparable to the separation between the rough lines in Fig. 4 (and Figs. 6 and 9 of [1]), so these rough lines are identified as those dislocation cell walls that destroy the coherence of x-ray diffraction between adjacent blocks of tempered martensite. The more diffuse dislocation distribution seen in Fig. 9 of ref. [1] would also be responsible for such a reduction in the mean size of diffraction domains, but the complexity of this dislocation distribution impairs the quantitative analysis of XRD peak broadenings.

Very much like for martensite, XRD data for austenite show a significant reduction in the average size of diffraction domains after cold rolling or overtempering (see Fig. 3). We believe that the formation of dislocation structures in the austenite is at least partially responsible for this reduction. The TEM images of the remaining austenite in Fig. 4 may show some defect structure. In addition, the background contrast in the TEM image of the austenite in Fig. 15 of ref. [1] changes between its left and right sides, suggesting a region of crystallographic disregistry in the center of the particle.

In general the quality of our x-ray data does not justify the decomposition of line profiles into two components, one component due to highly dislocated material in the dislocation cell walls, and the other component due to material in the cell interiors [11]. For cold-rolled material, however, the  $(211)\alpha'$  diffraction peak of Fig. 1c shows an asymmetry that suggests a two-component decomposition. This asymmetry from  $(211)\alpha'$  planes parallel to the plane of rolling is qualitatively consistent with the Poisson contraction of the material in the dislocation walls, as suggested by Ungar, et al. for copper tensile specimens [11]. (Our rolling direction was perpendicular to the diffraction vector.) Evidently this asymmetry does not arise because the fresh martensite has a smaller lattice parameter than the tempered martensite; the broad  $(211)\alpha'$  peaks from overtempered but unrolled material (Fig. 1c) are symmetric.

#### IV. DISCUSSION

We seek to understand why the austenite stability is reduced with tempering time. As described in [1], the reductions in austenite carbon concentrations during the first 81 hrs of tempering are too small to fully account for the observed loss of austenite stability. The increasing nickel concentration of the austenite during tempering [12] is a source of austenite stability that is evidently overcome by other effects on austenite stability. The other microstructural change discussed in [1] which may affect the austenite stability is the reduced coherency of the austenite/martensite interface, but the energetics of this coherency loss are probably small, and its role in the martensitic transformation is unclear.

In the following discussion we consider the dislocation structures that are formed around the transforming austenite particles. The energies associated with their formation are large enough to affect the thermodynamics of the transformation of the austenite particle. Changes in these defect structures during tempering result in changes of the "mechanical stability" of the austenite particles.

Without the formation and movement of dislocations around the transforming austenite particles, the local elastic stresses would become enormous, and would impede the transformation\*. The austenite particles would then be "mechanically stabilized" against the martensitic transformation. We propose that the relative difficulty of the plastic accommodation of a transforming austenite particle is the source of the "mechanical stability" of precipitated austenite in 9Ni steel. In the next section we show that the changes in "mechanical stability" which result from changes in the dislocation structure around the transforming particles can be large enough to account for the changes in austenite stability during isothermal tempering.

We have observed a dense dislocation structure around the surfaces of fresh martensite particles of many different sizes. That much of the plastic accommodation occurs near the fresh martensite / tempered martensite interface is reasonable because the stresses will be largest close to the transforming particle, and the interface has already been weakened by interface dislocations. Presumably the dislocations remain near the interface because they tangle soon after they are formed. The amount of plastic strain provided by the dislocation motion (i.e. the mean free path) needed to accommodate the transformation of an austenite particle scales with the volume of the particle. We suggest that the

---

\* It is interesting to point out that the elastic stresses that accompany the transformation probably do not affect the stability of the austenite particles as they grow larger. Since the transformation strains are so large, they must be primarily accommodated by plastic strains. Only a small fraction of the transformation strain energy remains as elastic energy. Furthermore, the residual elastic energy should tend to scale with the volume of the transformed particle. Therefore the small elastic energy barrier per volume of transformed particle should not change with tempering time.

increase in the number of dislocations times their Burgers vector and surface dislocation structure would not be so effective in accommodating the transformation of large particles because the number of dislocations in it times the length they have moved probably scales with the surface area of the particle.

Instead, when there is a transformation of austenite particles larger than about 0.5  $\mu\text{m}$ , it appears that more slip occurs in the tempered martensite away from the transforming particle. This slip involves a longer mean free path for each generated dislocation. A given amount of strain therefore requires fewer dislocations and a lower total energy expenditure for their formation. This formation energy is an important part of the energy required for plastic deformation, so as the austenite particles grow larger, the specific energy required to accommodate the transformation strains is reduced.

We can estimate effects on the thermodynamics of the transformation that result from a change in the type of transformation-induced dislocation structures. A high energy of formation is associated with the dense surface dislocation entanglements around transformed particles. Assuming a dislocation density of  $10^{13}/\text{cm}^2$  and an energy of 2 eV per atomic length of dislocation line, then if these entanglements occupy 10% of the bulk material when 10% of the material has freshly transformed to martensite, an energy of 0.01 eV/atom must be subtracted from the free energy difference that drives the transformation of the austenite particles. If we follow the Clausius-Clapeyron derivation for the equilibrium temperature of two phases [13], we expect a shift in the  $M_D$  temperature,  $\Delta T$ , of:

$$\Delta T = - \frac{(0.01 \text{ eV}) \cdot M_D}{L} \quad 6)$$

Using a value for the latent heat,  $L$ , of 0.02 eV/atom [14-17], we find a change in  $M_D$  of at least -150 K associated with the formation of the surface dislocation structure around the transformed particles.

The more extended type of dislocation structure in the tempered martensite should require less formation energy to accommodate a given transformed volume. When the transformation is accommodated by this more extended dislocation structure,  $M_D$  will not be so strongly suppressed. It seems plausible that the changes in defect structures around larger transforming particles can cause  $M_D$  to increase by more than 100 K. In essence, the austenite stability is reduced as the particles grow larger because the accommodation of the transformation strains apparently requires less energy. Additionally, for the dense dislocation entanglements around the transformed particles some of the formation energy probably scales with the surface area of the particle. As the austenite particles grow larger this surface energy barrier becomes less important, so the austenite particles will lose stability with increased tempering time.

## V. SUMMARY AND CONCLUSIONS

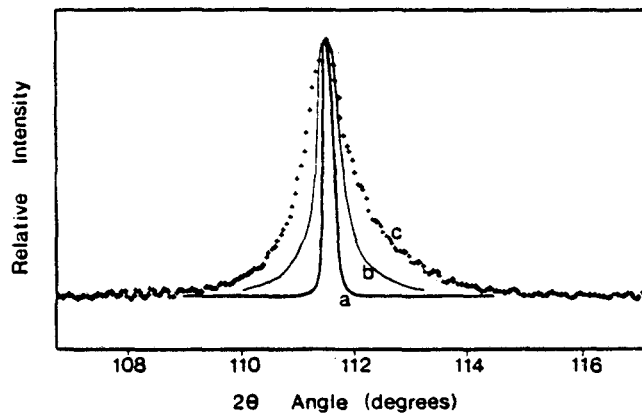
The "mechanical stability" of austenite particles is based on the energy associated with the accommodation of the transformation strains. In conjunction with TEM observations, the large changes in x-ray line profiles of both the austenite and martensite phases show a dramatic rise in dislocation densities when some of the austenite transforms to martensite. These high dislocation densities result from the large transformation strains. The net energy required to create and move these dislocations will depend on characteristics of the dislocation structure; primarily the number of dislocations and their arrangement. The different nature of the dislocation structures which form around small and around large transforming austenite particles are responsible for the change in "mechanical stability" of austenite particles as they grow larger. We have observed that dislocations around large transformed particles have moved further into the surrounding tempered martensite, and we suggest that these structures provide strain accommodation with fewer dislocations. So when larger particles transform, less energy is required to generate the dislocations which accommodate the transformation, and the transformation proceeds more easily. In addition, we suggest that the loss of stability of the austenite as it grows could also be due to a scaling of some energy in the dislocation structure with the surface/volume ratio of the austenite particles. Both these changes in the dislocation structures around transforming austenite particles should reduce the "mechanical stability" of austenite particles as they grow larger during isothermal tempering.

## ACKNOWLEDGMENTS

The authors are grateful to Drs. J.I. Kim, Y.H. Kim, H.J. Kim and G.O. Fior for important discussions. This work was supported by the Director, Office of Basic Energy Science, Materials Science Division of the U. S. Department of Energy under contract no. DE-AC03-76SF00098.

REFERENCES

1. B. Fultz, J.I. Kim, Y.H. Kim, H.J. Kim, G.O. Fior and J.W. Morris, Jr.: Met. Trans. A in press.
2. B.E. Warren and B.L. Averbach: J. Appl. Phys., 1950, vol. 21, p. 595.
3. B.E. Warren: X-Ray Diffraction, Chap. 13, Addison-Wesley, Reading, Mass., 1969.
4. B.E. Warren: Prog. Metal Phys., vol. 8, B. Chalmers and R. King, eds., 1959, Pergamon Press, New York, p. 159.
5. W.A. Rachinger: J. Sci. Instr., 1948, vol. 25, p. 254.
6. A.R. Stokes: Proc. Phys. Soc. London, 1948, vol. 61, p. 382.
7. A.G. Khachatryan: Sov. Phys. Cryst., 1960, vol. 5, p. 335.
8. M. Wilkens: Phys. Stat. Solidi, 1970, vol. 2, p. 359.
9. M.A. Krivoglaz and K.P. Ryaboshapka: Fiz. Metal. Metalloved., 1963, vol. 15, p. 18.
10. S.I. Kwun and R.A. Fournelle: Met. Trans. A, 1980, vol. 11, p. 1429.
11. T. Ungar, H. Mughrabi, D. Ronnpagel and M. Wilkens: Acta Metall., 1984, vol. 32, p. 333.
12. B. Fultz, J.I. Kim and J.W. Morris, Jr: unpublished research, 1985.
13. C. Kittel: Thermal Physics, 1969, John Wiley, New York, p. 327.
14. L. Kaufman and M. Cohen: Prog. Metal Phys., 1958, vol. 7, B. Chalmers and R. King, eds., Pergamon Press, New York, p. 165.
15. M.A. Krivoglaz and V.D. Sadovskiy: Fiz. Metal. Metalloved., 1964, vol. 18, p. 23.
16. L.V. Voronchikhin and I.G. Fakidov: Fiz. Metal. Metalloved., 1976, vol. 21, p. 119.
17. E.I. Estrin: Fiz. Metal. Metalloved., 1975, vol. 19, p. 119.



XBL 842-599

Fig. 1. Representative Rachinger and Stokes corrected (211)<sub>a'</sub> XRD peaks from 9 Ni steel. a) dark line: 9 hr tempering at 590°C, quench to 0°C. b) light line: 240 hr tempering at 590°C, quench to 0°C. c) crosses: 240 hr tempering at 590°C, quench to 0°C, 75% cold rolling.

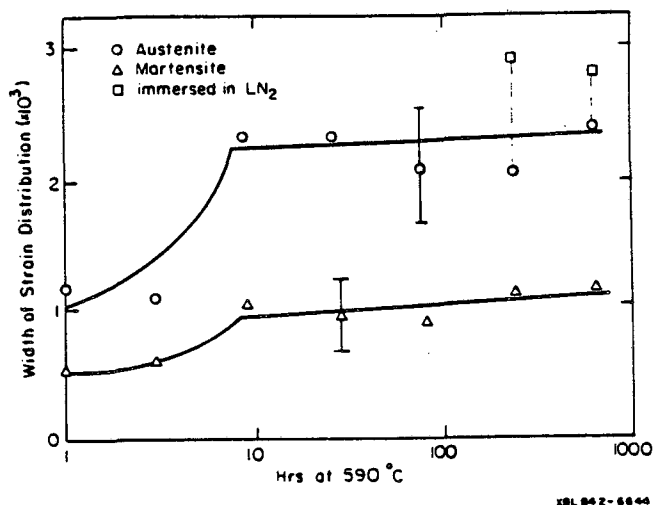


Fig. 2. Full-width-at-half-maximum of the strain distribution versus tempering time at  $590^\circ\text{C}$ . Circle: austenite; peak up triangle: martensite; square: austenite immersed in liquid nitrogen.

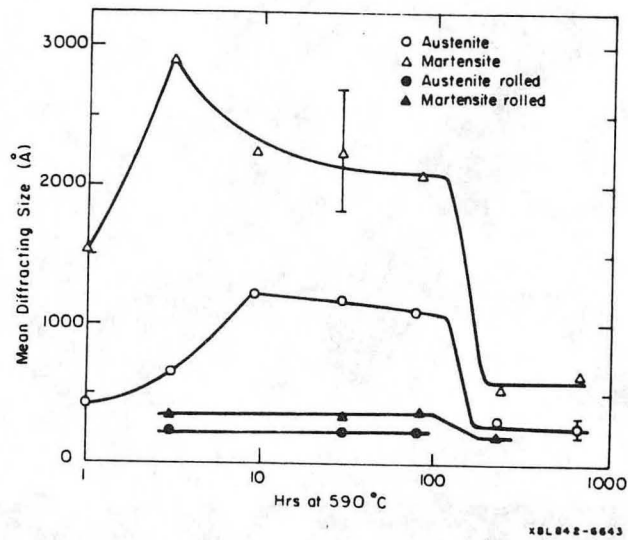
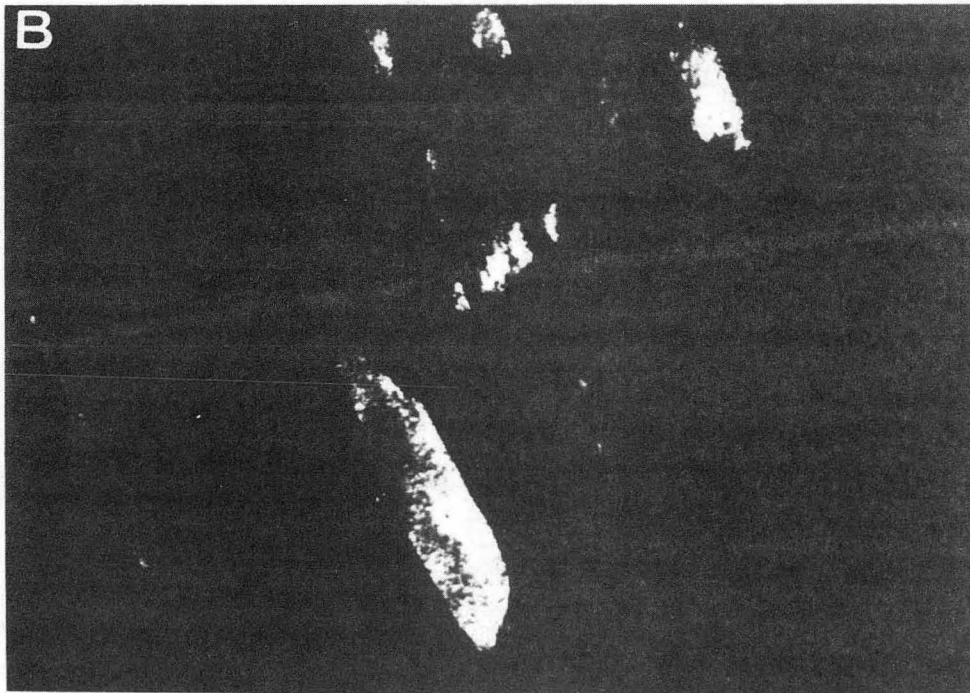
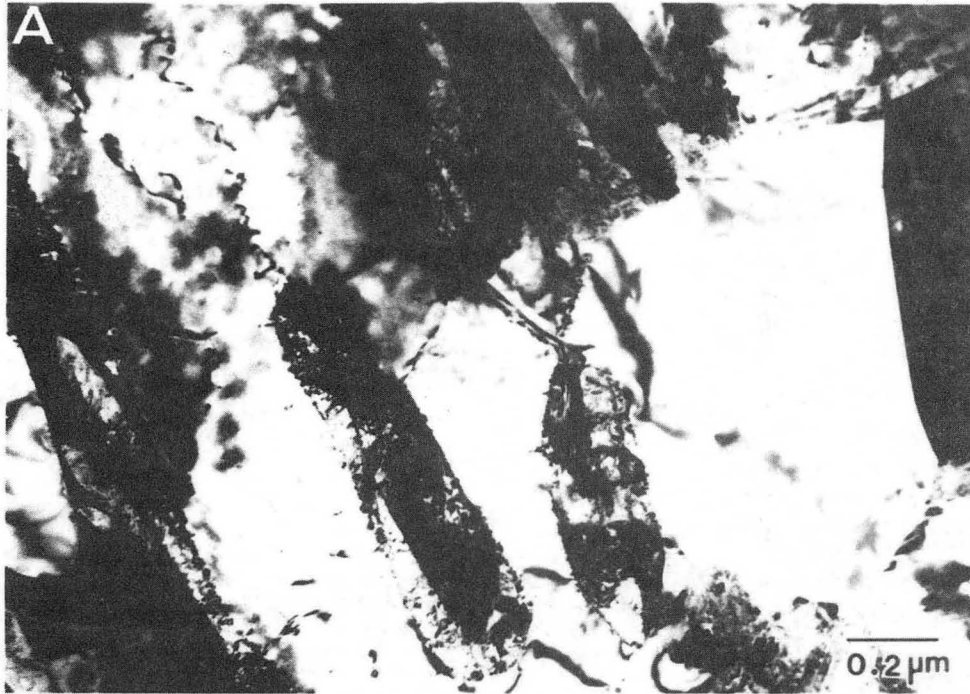
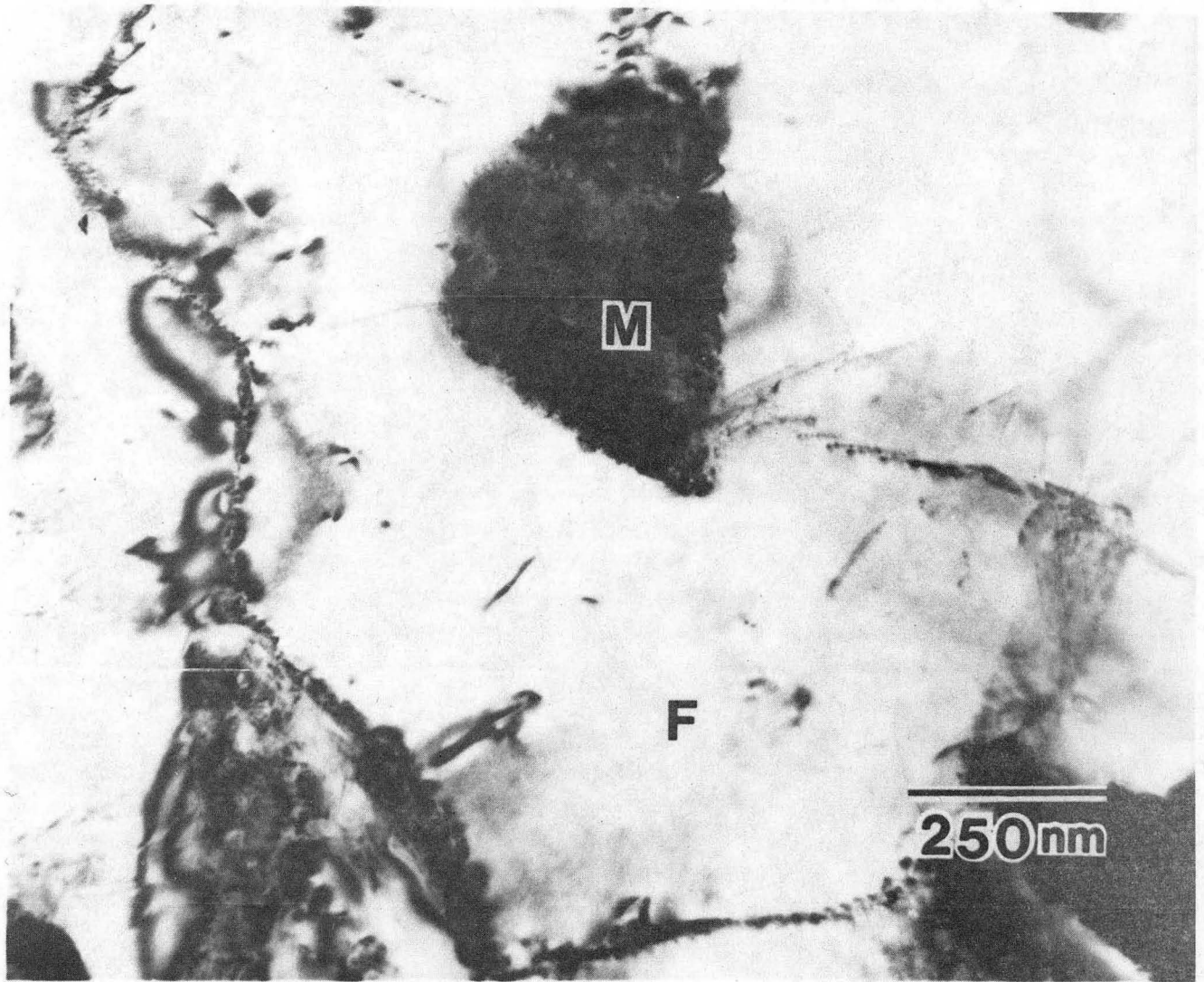


Fig. 3. Mean size of coherently diffracting domains versus tempering time at 590°C. Circle: austenite quenched to 0°C; triangle: martensite quenched to 0°C; solid circle: austenite after 75% cold rolling; solid triangle: martensite after 75% cold rolling.



XBB 840-8780

Fig. 4 TEM micrographs of 9 Ni steel tempered for 300 hrs at 590°C.  
A: bright field B: dark field of 002γ



XBB 835-4181A

Fig. 5. Bright field TEM micrograph of 9Ni steel tempered 81 hrs at 590°C.



XBB 844-2630

Fig. 6. Bright field TEM micrograph of fresh and tempered martensite in 9 Ni steel tempered 3 hrs at 590°C followed by 25% cold rolling.

This report was done with support from the Department of Energy. Any conclusions or opinions expressed in this report represent solely those of the author(s) and not necessarily those of The Regents of the University of California, the Lawrence Berkeley Laboratory or the Department of Energy.

Reference to a company or product name does not imply approval or recommendation of the product by the University of California or the U.S. Department of Energy to the exclusion of others that may be suitable.

*LAWRENCE BERKELEY LABORATORY  
TECHNICAL INFORMATION DEPARTMENT  
UNIVERSITY OF CALIFORNIA  
BERKELEY, CALIFORNIA 94720*